Original Article

Enhancing prediction of cervical lymph node metastasis in papillary thyroid carcinoma through nodule-oriented quantification: combined S-Detect and ultrasound elastography

Ze-Lin Xu[1#], Ji-Xue Hou[2#], Zhen-Hao Zheng[1], Ya-Qian Deng[1], Guan-Ming Zeng[3], Si-Rui Wang[1], Pei-Shan Zhu[1], Yan-Fei Kang[1], Ting-Ting Du[1], Jian Dong[1], Wen Liu[1], Jun Li[1,4], Xin-Wu Cui[5]

[1]Department of Ultrasound, the First Affiliated Hospital of Shihezi University, Shihezi, China; [2]Department of Thyroid and Breast Surgery, the First Affiliated Hospital of Shihezi University, Shihezi, China; [3]Department of Imaging Center, the First Affiliated Hospital of Shihezi University, Shihezi, China; [4]National Health Commission Key Laboratory of Prevention and Treatment of Central Asia High Incidence Diseases, First Affiliated Hospital, School of Shihezi University, Shihezi, China; [5]Department of Medical Ultrasound, Tongji Hospital, Tongji Medical College, Huazhong University of Science and Technology, Wuhan, China

Contributions: (I) Conception and design: ZL Xu, JX Hou; (II) Administrative support: J Li, XW Cui; (III) Provision of study materials or patients: ZL Xu, ZH Zheng, YQ Deng; (IV) Collection and assembly of data: JX Hou, ZH Zheng, YF Kang, TT Du, J Dong; (V) Data analysis and interpretation: ZL Xu, YQ Deng, GM Zeng, SR Wang, PS Zhu, W Liu; (VI) Manuscript writing: All authors; (VII) Final approval of manuscript: All authors.

[#]These authors contributed equally to this work as co-first authors.

Correspondence to: Jun Li, MD. Department of Ultrasound, the First Affiliated Hospital of Shihezi University, 107 North Second Road, Shihezi 832008, China; National Health Commission Key Laboratory of Prevention and Treatment of Central Asia High Incidence Diseases, First Affiliated Hospital, School of Shihezi University, Shihezi, China. Email: 1287424798@qq.com; Xin-Wu Cui, MD. Department of Medical Ultrasound, Tongji Hospital, Tongji Medical College, Huazhong University of Science and Technology, 1095 Jiefang Avenue, Wuhan 430030, China. Email: cuixinwu@live.cn.

Background: Papillary thyroid carcinoma (PTC) frequently metastasizes to cervical lymph nodes (LNs), with metastasis rates of 20–90%, significantly impacting patient prognosis. Although ultrasound (US) is the primary preoperative assessment tool, its accuracy (Acc) in detecting LN metastasis (LNM) remains insufficient, with conventional US detecting only 50% of confirmed cases. This study aimed to improve the prediction of cervical LNM in PTC by combining quantitative nodule orientation parameters with multi-modal US techniques.

Methods: Data were retrospectively collected from 117 patients (141 nodules: 85 non-metastasis and 56 metastasis) who underwent PTC resection and cervical LN dissection from September 2023 to May 2024. All patients underwent US, US elastography (UE), and S-Detect examinations before surgery. For each nodule, the angle between the nodule's maximum diameter and the skin was measured. Logistic regression analysis assessed the correlation between each variable and cervical LNM, identified significant predictive factors, and a predictive model presented as a nomogram was constructed.

Results: Univariate analysis showed significant differences between non-metastasis and metastasis groups in orientation quantification [–9.3° (–35.2°, 17.2°) *vs.* 13.9° (–1.6°, 54.0°), P<0.001], age (P=0.002), maximum nodule diameter (P=0.017), boundary (P=0.021), microcalcifications on S-Detect (P=0.014), microcalcifications (P=0.036), and ECI scores (P=0.043). Multivariate analysis identified seven independent predictors for cervical LNM, with S-Detect-detected microcalcifications showing the highest odds ratio (OR) [OR =4.159; 95% confidence interval (CI): 1.545–11.199]. The combined predictive model incorporating conventional US, UE, S-Detect, and orientation quantification demonstrated superior diagnostic performance [area under the curve (AUC) =0.861; 95% CI: 0.803–0.919] compared to individual models

(P<0.001), achieving sensitivity (Sen) of 0.911 and specificity (Spe) of 0.659. The nomogram showed good calibration with no significant deviation (χ^2=3.271; P=0.926).

Conclusions: S-Detect accurately identifies the direction of the maximum diameter of thyroid nodules, and quantification of the longitudinal section orientation can be used as an independent predictor for LNM in PTC.

Keywords: Ultrasonography; diagnostic imaging; thyroid nodule; lymphatic metastasis

Submitted Aug 10, 2024. Accepted for publication Feb 23, 2025. Published online Mar 28, 2025.
doi: 10.21037/qims-24-1650
View this article at: https://dx.doi.org/10.21037/qims-24-1650

Introduction

In recent years, extensive statistical data have indicated that the incidence of thyroid cancer remains high among populations both domestically and internationally (1-3). Papillary thyroid carcinoma (PTC) is the primary contributor to overall thyroid cancer and is the only histological subtype that has systematically increased in all countries, despite significant disparities between nations. PTC frequently metastasizes to the cervical lymph nodes (LNs), with central LN metastasis (CLNM) rates reaching as high as 20% to 90%. Cervical LN metastasis (LNM) not only significantly increases the risk of disease recurrence but also adversely affects survival rates (4). Therefore, accurate preoperative evaluation of cervical LNM is crucial for tumor staging, treatment planning, and prognosis (5).

Ultrasound (US), as a necessary examination for patients with suspected thyroid nodules and for the preoperative assessment of thyroid cancer, has advantages such as real-time imaging, non-invasiveness, and multifunctionality (6,7). Nevertheless, conventional US demonstrates limited sensitivity (Sen) in detecting metastatic LNs in thyroid cancer, identifying only approximately 50% of surgically confirmed cases (8). US elastography (UE) analyzes the stiffness of thyroid nodules, providing qualitative, semi-quantitative, and quantitative parameters that assist in differentiating between benign and malignant nodules (9). In numerous publications, UE has demonstrated good performance in identifying the malignancy of suspicious thyroid nodules, particularly for PTC (10,11). However, the value of UE parameters in predicting cervical LNM for PTC nodules remains a topic of debate (12,13).

Conventional US relies heavily on subjective judgment, which has prompted the integration of artificial intelligence (AI)-based computer-aided diagnosis (CAD) systems for thyroid nodules in clinical practice (14). AI can extract and quantify key image information, converting image diagnosis from a subjective qualitative analysis to a more objective quantitative analysis. S-Detect stands as the most extensively validated CAD system in thyroid nodule US evaluation (15,16). However, its primary application has been in differentiating benign from malignant nodules, with limited research exploring its predictive value for LNM in thyroid cancer.

Numerous studies have suggested that the non-parallel orientation of thyroid nodules constitutes an essential feature for evaluating the risk of malignant tumor metastasis and is widely utilized in clinical practice per the Thyroid Imaging Reporting and Data System (TI-RADS) guidelines (7,17-20), which closely link neck LNM with a poor prognosis. The predictive value of an aspect ratio >1 in predicting cervical LNM in PTC has been confirmed in several studies (21,22) and incorporated as a factor in machine learning models (23). Among these criteria, aspect ratio >1 is acknowledged as the primary indicator for determining nodule orientation. However, it merely measures a simple visual assessment of the maximum longitudinal and transverse diameters in a particular plane, which may not represent the nodule's genuine maximum growth direction. This subjective binary classification gives rise to concerns regarding its accuracy (Acc). Therefore, establishing threshold definitions for growth direction and precise quantitative standards for parallel and non-parallel orientations would ensure greater scientific rigor. In this paper, direction quantification will be explored and analyzed as a potential independent predictive factor. We aim to conduct a comprehensive analysis to investigate the role of quantitative orientational parameters in predicting cervical LNM in PTC and particularly assess their value as independent predictive factors.

Considering the limitations in Sen and the challenges inherent in predicting LNM, this study endeavors

to investigate the Acc of predicting cervical LNM in PTC patients. We achieve this by precisely quantifying the orientation characteristics of thyroid nodules and integrating advanced UE and S-Detect. Studies have demonstrated that multi-modal US exhibits superior predictive performance compared to conventional single-mode US, with the triple-modality model achieving the area under the curve (AUC) with 95% confidence interval (CI) of 0.831 (0.812, 0.850) (24). Our goal is to provide more precise and scientific evidence for the clinical diagnosis and treatment of thyroid diseases, ultimately reducing the risk of PTC recurrence and improving patient prognosis. We present this article in accordance with the STROBE reporting checklist (available at https://qims.amegroups.com/article/view/10.21037/qims-24-1650/rc).

Methods

Study design and patients

This study aims to develop a predictive model for LNM in PTC by integrating S-Detect, UE, and directional quantitative analysis. The estimated minimum sample size required by the events per variable (EPV) method is 60 (25). A retrospective analysis was conducted on 117 patients (with a total of 141 nodules) who underwent thyroid cancer resection and neck LN dissection at the First Affiliated Hospital of Shihezi University from September 2023 to May 2024. The gold standard for identifying LNM was based on the postoperative paraffin pathology results. The study was conducted in accordance with the Declaration of Helsinki (as revised in 2013). The study was approved by the institutional ethics committee of the First Affiliated Hospital of Shihezi University (No. KJ2024-250-01). Informed consent was taken from all the participants.

Inclusion criteria: (I) complete baseline clinical data; (II) underwent conventional US, UE (E-thyroid), and S-Detect examinations within 1 week before surgery; (III) no history of neck radiation or thyroid surgery; and (IV) paraffin-embedded pathological diagnosis of PTC.

Exclusion criteria: (I) subjects with large calcifications within the nodule (or those accompanied by significant shadowing), rendering it impossible to fully visualize the nodule; (II) subjects who did not undergo surgery at this hospital and whose intraoperative LN dissection status was not recorded; (III) subjects with thyroid lesions display no discernible mass and unclear margins on US examination; and (IV) subjects with diffuse thyroid disease or a history of other malignant neoplasms.

Conventional US and S-Detect examination

The SAMSUNG RS85 and RS80 color Doppler US diagnostic instruments (equipped with an L3–12A probe, frequency 5–13 MHz), equipped with S-Detect computer-aided diagnostic analysis software and UE technology, were used to instruct to adopt the supine position, fully exposing the neck, first perform routine scanning of the thyroid and cervical LNs, subsequently followed by a comprehensive multi-plane examination of the thyroid nodule. The images were scrutinized by two US physicians with more than 5 years of experience, observing and recording key features of the nodules, such as the maximum diameter, location, aspect ratio, boundary, edges, calcification, internal echoes, and other sonographic characteristics.

Adjust the image, select the transverse and longitudinal planes with the most malignant features of the lesion as the standard planes, freeze the image, activate the S-Detect mode, which automatically identifies the sonographic features of the lesion, including composition, echo intensity, orientation, shape, calcification, and edges, and records the binary classification results.

E-thyroid examination

Fix on the maximum longitudinal section of the target nodule, initiate the elasticity contrast index (ECI) program (26), ensure that the sampling frame covers an area larger than the lesion, instruct the patient to hold their breath and avoid swallowing, and wait until the elastic image color bar shows all green, which indicates a successful detection.

At this juncture, freeze the image, based on the elasticity scores (4-point method, ES), manually delineate the lesion edges to derive the semi-quantitative ECI value (27). Measure the ECI value of each nodule 3 to 5 times and take the average. The obtained ECI value represents the homogeneity within the lesion.

All examinations were performed by two experienced and proficient US diagnostic physicians.

Quantifying the orientation

Orientation quantification was performed utilizing conventional US and S-Detect, and angle measurement was done through Adobe Photoshop 2023. Based on

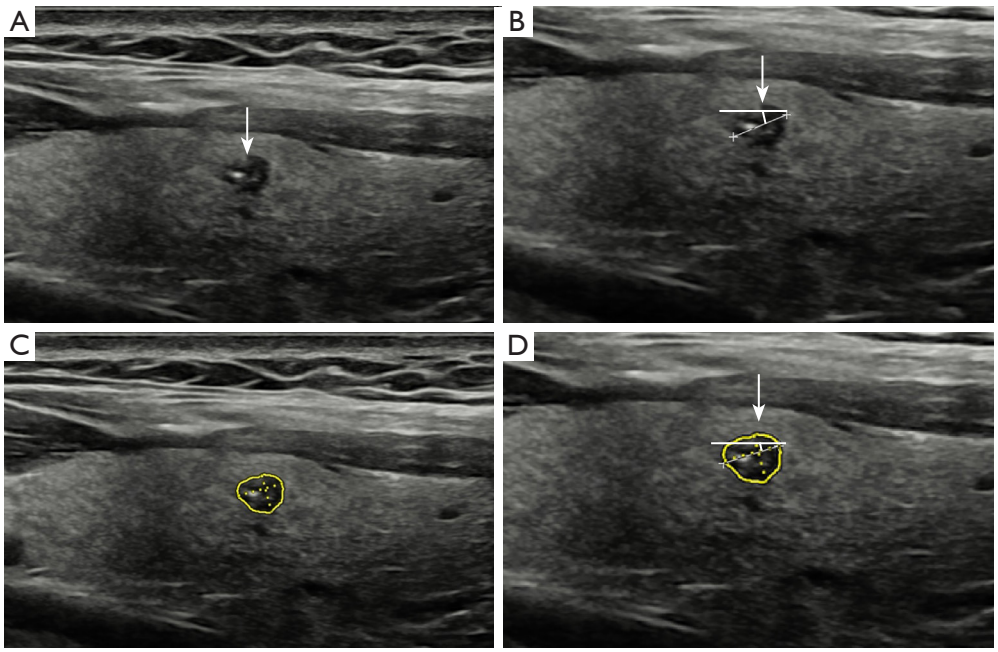

Figure 1 A 49-year-old male patient with PTC has a nodule located in the middle part of the left lobe. The maximum diameter of the nodule is tilted towards the head. Tilts towards the head are considered negative. (A) Conventional US in the longitudinal plane (the arrow points to the nodule). (B) The angle measured in the longitudinal plane by conventional US is −22.1° (the arrow points to the angle measurement pattern of the nodule). (C) S-Detect in the longitudinal plane. The yellow circle represents the nodule ROI region automatically outlined by S-Detect. (D) The angle measured in the longitudinal plane by S-Detect is −17.1° (arrows). The yellow circle represents the nodule ROI region automatically outlined by S-Detect. PTC, papillary thyroid carcinoma; ROI, region of interest; US, ultrasound.

conventional US and S-Detect examinations, transverse and longitudinal section images were obtained, defining the angle as the acute angle formed between the maximum diameter of the nodule and the skin within the indicated plane (range, 0–90 degrees). This angle was assigned a positive value for directions orienting towards the patient's right side and upper side, and a negative value for directions towards the left side and lower side, with the measured angles recorded accordingly (*Figure 1*). Additionally, each measured angle value was subjected to the following two quantification conversions and recorded:

(I) Absolute value conversion: record the absolute value of the angle.

(II) Ipsilateral positional conversion value: according to the location of the nodule (a total of 132 nodules) within the lobe, angles marked by the acute angle on the same side are positive, and those on the opposite side are negative.

The angle measurements were independently conducted by two physicians, and the average values of their measurements were taken. Where there was a significant disagreement in the maximum diameter direction, or if the directions were completely opposite, the two physicians would negotiate until consensus was reached.

Statistical analysis

This study conducted a systematic statistical analysis using the R language (R 4.3.3). Initially, all continuous variables were examined through a normality test. For variables that adhered to a normal distribution, they were described with the mean ± standard deviation; otherwise, the median (interquartile range) was used. Subsequently, significant variables were identified using univariate logistic regression analysis, followed by the determination of cutoff values for important continuous variables. To prevent overfitting, correlation coefficients were analyzed to examine multicollinearity among significant variables. Inter-rater agreement and intra-rater reliability were determined with an intraclass correlation coefficient (ICC). Thereafter,

Table 1 Results of the concordance analysis for the longitudinal and transverse plane measurements obtained by two different physicians using conventional US and S-Detect orientational quantification angles

Measuring physician	Transverse section		Longitudinal section	
	Conventional US (°)	S-Detect (°)	Conventional US (°)	S-Detect (°)
1	–1.4 (–56.8, 53.4)	11.2 (–21.5, 49.9)	4.0 (–52.5, 53.2)	6.5 (–21.2, 25.8)
2	0.4 (–52.5, 53.2)	11.2 (–21.5, 50.3)	2.9 (–41.8, 26.9)	6.5 (–21.4, 25.8)
ICC (95% CI)	0.991 (0.987–0.993)	0.999 (0.999–0.999)	0.984 (0.978–0.989)	0.999 (0.999–0.999)

Nonnormally distributed data are expressed as median (interquartile range). CI, confidence interval; ICC, intraclass correlation coefficient; US, ultrasound.

multivariate logistic regression analysis was performed to identify independent predictors and to assess the role of orientational quantification in predicting LNM in PTC. A nomogram model was developed and evaluated for stability using 10-fold cross-validation. Furthermore, the receiver operating characteristic (ROC) curves were plotted for conventional US, orientational quantification, S-Detect, and ECI scores, as well as for the overall model, DeLong's test was applied to compare the AUC of these models. To assess the model's predictive Acc, calibration curves, and decision analysis curves for the best predictive model were plotted. Statistical significance was defined as P<0.05.

Results

Sample of the study

Within the 141 thyroid nodules, 85 were in the non-metastasis group, and 56 were in the metastasis group (49.21±10.25 years; 59 males). Specifically, in the metastasis group, 54 patients had CLNM, 13 had non-central LNM, and only one case involved extensive metastasis (defined as >5 metastatic LNs) (28).

Outcome of statistical analysis

The ICC for the quantification angles of thyroid nodules in transverse and longitudinal sections, as measured by two different physicians using both conventional US and S-Detect methods, was consistently above 0.98 (*Table 1*), indicating a high degree of consistency. Additionally, the direction quantification angles of the maximum diameter in the longitudinal section of S-Detect for the non-metastasis and metastasis groups of thyroid nodules were –9.3° (–35.2°, 17.2°) and 13.9° (–1.6°, 54.0°), respectively, with a statistically significant difference (P<0.001). Further analysis through univariate logistic regression revealed significant differences in age (P=0.002), maximum diameter of the nodule (P=0.017), boundary (P=0.021), microcalcifications (P=0.036), microcalcifications identified in the longitudinal section of S-Detect (P=0.014), and ECI scores (P=0.043) between the metastasis and non-metastasis groups (*Tables 2-4*). Similarly, multivariate logistic regression analysis indicated that age, maximum diameter of the nodule, boundary, direction quantification angle of the maximum diameter of thyroid nodules identified by S-Detect, microcalcifications identified in the longitudinal section of S-Detect, and ECI scores were independent predictors of cervical LNM (*Table 5*). The cut-off value for the direction quantification angle was –16.35°, with Sen, specificity (Spe), positive predictive value (PPV), negative predictive value (NPV), Acc, and AUC for predicting cervical LNM in PTC of 0.929, 0.471, 0.536, 0.909, 0.652, 0.688 (P<0.001; 95% CI: 0.601–0.776), respectively. Notably, the microcalcifications identified in the longitudinal section of S-Detect were the best predictors for the metastasis group, with an odds ratio (OR) of 4.159 (95% CI: 1.545–11.199). Moreover, correlation coefficient testing revealed no significant overfitting among the seven independent predictors selected by multivariate logistic regression (correlation coefficients all <0.3) (*Figure 2*). As shown in Table S1, compared to using US alone, orientation quantification improved diagnostic PPV, NPV, and Acc. In comparison, compared to using conventional US, UE, S-Detect, and orientation quantification alone, the combined predictive model had Sen, Spe, PPV, NPV, Acc, and AUC of 0.911, 0.659, 0.637, 0.918, 0.759, 0.861 (95% CI: 0.803–0.919), respectively, indicating high overall predictive capability. The DeLong's test results demonstrate that the combined predictive model significantly outperforms all individual models (P<0.001 for all comparisons). Specifically, the Z-value indicates that the

Table 2 Univariate analysis of conventional US for cervical LNM in PTC patients

Characteristics	Overall	Non-metastasis	Metastasis	P
Age (years)	51.0 (45.0, 57.0)	52.0 (46.0, 57.0)	50.0 (44.8, 56.0)	0.377
Age				0.002
<55 years	53 (37.6)	23 (27.1)	30 (53.6)	
≥55 years	88 (62.4)	62 (72.9)	26 (46.4)	
Gender				0.397
Female	82 (58.2)	47 (55.3)	35 (62.5)	
Male	59 (41.8)	38 (44.7)	21 (37.5)	
Weight (kg)	67.0 (61.0, 72.0)	68.0 (62.0, 72.0)	64.0 (60.0, 70.0)	0.709
Height (cm)	166.0 (159.0, 170.0)	166.0 (160.0, 170.0)	166.5 (158.8, 170.3)	0.893
ECI	1.94 (1.35)	1.83 (1.38)	2.10 (1.29)	0.243
ECI scores				0.043
1	53 (37.6)	42 (49.4)	11 (19.6)	
2	54 (38.3)	33 (38.8)	21 (37.5)	
3	19 (13.5)	6 (7.1)	13 (23.2)	
4	15 (10.6)	4 (4.7)	11 (19.6)	
Nodule size (cm)	0.89 (0.59, 1.19)	0.72 (0.55, 1.00)	0.99 (0.68, 1.33)	0.015
Nodule size				0.017
<1 cm	97 (68.8)	65 (76.5)	32 (57.1)	
≥1 cm	44 (31.2)	20 (23.5)	24 (42.9)	
Echogenicity				0.266
Hyperechoic/isoechoic	6 (4.3)	5 (5.9)	1 (1.8)	
Hypoechoic	135 (95.7)	80 (94.1)	55 (98.2)	
Orientation				0.276
Horizontal	43 (30.5)	23 (27.1)	20 (35.7)	
Vertical	98 (69.5)	62 (72.9)	36 (64.3)	
Boundary				0.021
Clear	106 (75.2)	78 (91.8)	28 (50.0)	
Obscure	35 (24.8)	7 (8.2)	28 (50.0)	
Margin				0.620
Smooth	128 (90.8)	78 (91.8)	50 (89.3)	
Irregular	13 (9.2)	7 (8.2)	6 (10.7)	
Microcalcifications				0.036
No	102 (72.3)	67 (78.8)	35 (62.5)	
Yes	39 (27.7)	18 (21.2)	21 (37.5)	
Composition				0.862
Cystic or solid-cystic	7 (5.0)	4 (4.7)	3 (5.4)	
Solid	134 (95.0)	81 (95.3)	53 (94.6)	

Continuous variables were expressed as median (interquartile range) for nonnormally distributed data. The normality of continuous variables was assessed using the Shapiro-Wilk test. Categorical variables were expressed as number (%). ECI, elasticity contrast index; LNM, lymph node metastasis; PTC, papillary thyroid carcinoma; US, ultrasound.

Table 3 Univariate analysis of S-Detect for cervical LNM in PTC patients

Characteristics	Transverse section				Longitudinal section			
	Overall	Non-metastasis	Metastasis	P	Overall	Non-metastasis	Metastasis	P
Binary recommendation				0.280				0.493
Possibly benign	13 (9.2)	6 (7.1)	7 (12.5)		10 (7.1)	5 (5.9)	5 (8.9)	
Possibly malignant	128 (90.8)	79 (92.9)	49 (87.5)		131 (92.9)	80 (94.1)	51 (91.1)	
Composition				0.103				0.638
Cystic or partially cystic	11 (7.8)	4 (4.7)	7 (12.5)		12 (8.5)	8 (9.4)	4 (7.1)	
Solid	130 (92.2)	81 (95.3)	49 (87.5)		129 (91.5)	77 (90.6)	52 (92.9)	
Echogenicity				0.185				0.862
Hyperechoic/isoechoic	10 (7.1)	4 (4.7)	6 (10.7)		7 (5.0)	4 (4.7)	3 (5.4)	
Hypoechoic	131 (92.9)	81 (95.3)	50 (89.3)		134 (95.0)	81 (95.3)	53 (94.6)	
Orientation				0.735				0.687
Parallel	78 (55.3)	48 (56.5)	30 (53.6)		98 (69.5)	58 (68.2)	40 (71.4)	
Non-parallel	63 (44.7)	37 (43.5)	26 (46.4)		43 (30.5)	27 (31.8)	16 (28.6)	
Shape				0.321				0.752
Ovoid to round	114 (80.9)	71 (83.5)	43 (76.8)		114 (80.9)	68 (80.0)	46 (82.1)	
Irregular	27 (19.1)	14 (16.5)	13 (23.2)		27 (19.1)	17 (20.0)	10 (17.9)	
Calcifications				0.303				0.014
No calcifications	78 (55.3)	50 (58.8)	28 (50.0)		66 (46.8)	47 (55.3)	19 (33.9)	
Microcalcifications	63 (44.7)	35 (41.2)	28 (50.0)		75 (53.2)	38 (44.7)	37 (66.1)	
Margin				0.065				0.238
Well-defined smooth	27 (19.1)	12 (14.1)	15 (26.8)		26 (18.4)	13 (15.3)	13 (23.2)	
Microlobulated/ spiculated/ill-defined	114 (80.9)	73 (85.9)	41 (73.2)		115 (81.6)	72 (84.7)	43 (76.8)	

The normality of continuous variables was assessed using the Shapiro-Wilk test. Categorical variables were expressed as number (%). LNM, lymph node metastasis; PTC, papillary thyroid carcinoma.

most notable difference is between the combined model and S-Detect (Z=5.732), which is aligning with the relatively low AUC of S-Detect (0.607). Among all individual models, the difference is least pronounced with the US model (Z=3.694), suggesting its performance is closer to that of the composite model, indicating the fundamental importance of conventional US features in the diagnostic process (Table S1). Subsequently, a nomogram was devised based on the results of the multivariate regression analysis (*Figures 3*,*4*). The calibration curves were in close agreement with the actual cervical LNM situation, with no statistically significant difference in the goodness-of-fit test (χ^2=3.271; P=0.926), further underscoring the model's good consistency (*Figure 5*).

Discussion

Several guidelines have indicated that an aspect ratio >1 is a highly specific but less sensitive indicator of malignancy (7,17-19). Nonetheless, a notable absence persists in terms of further recommendations specifically tailored for the assessment of obliquely oriented nodules. Research endeavors into the growth direction of thyroid cancer have predominantly focused on the microscopic molecular realm,

Table 4 Univariate analysis of orientation quantification for cervical LNM in PTC patients

Characteristics	Transverse section				Longitudinal section			
	Overall	Non-metastasis	Metastasis	P	Overall	Non-metastasis	Metastasis	P
Conventional US (°)	0.4 (–56.3, 56.7)	–2.6 (59.8, 52.9)	5.1 (51.0, 60.0)	0.362	4.1 (–42.4, 29.3)	2.1 (–36.0, 29.3)	6.1 (–25.9, 25.2)	0.632
ABV in US (°)	56.7 (25.9, 74.1)	56.2 (26.0, 76.1)	58.9 (25.2, 72.5)	0.923	32.2 (15.0, 68.8)	35.5 (16.4, 68.8)	26.5 (13.2, 68.6)	0.464
S-Detect (°)	11.2 (–21.5, 50.1)	11.9 (–20.9, 45.4)	75.6 (–23.9, 50.6)	0.627	6.5 (–21.3, 25.8)	–9.3 (–35.2, 17.2)	13.9 (–1.6, 54.0)	<0.001
ABV in S-Detect (°)	32.5 (15.5, 67.5)	30.3 (15.9, 69.9)	39.5 (13.2, 67.2)	0.957	22.5 (11.1, 62.8)	25.0 (12.7, 62.8)	17.6 (8.0, 63.7)	0.485
Conversion in S-Detect				0.684				0.147
Parallel	60 (42.6)	35 (41.2)	25 (44.6)		66 (46.8)	44 (51.8)	22 (39.3)	
Non-parallel	81 (57.4)	50 (58.8)	31 (55.4)		75 (53.2)	41 (48.2)	34 (60.7)	

Continuous variables were expressed as median (interquartile range) for nonnormally distributed data. The normality of continuous variables was assessed using the Shapiro-Wilk test. Categorical variables were expressed as number (%). ABV, absolute binocular vision; LNM, lymph node metastasis; PTC, papillary thyroid carcinoma; US, ultrasound.

Table 5 Logistic regression analysis of risk factors for cervical LNM in PTC

Variables	Estimate	Std	Z value	P	OR (95% CI)
Boundary in US (obscure)	1.692	0.536	3.159	0.002	5.432 (1.901–15.521)
Age (<55 years)	–1.243	0.462	–2.691	0.007	3.465 (1.402–8.565)
Nodule size (≥1 cm)	1.265	0.513	2.467	0.014	3.543 (1.297–9.676)
Calcifications in US (microcalcifications)	0.585	0.494	1.184	0.236	1.795 (0.682–4.727)
Calcifications in SD-LS (microcalcifications)	1.425	0.505	2.820	0.005	4.159 (1.545–11.199)
ECI scores (ES3/ES4)	1.023	0.251	4.068	<0.001	2.781 (1.699–4.552)
Orientation quantification in SD-LS	0.014	0.006	2.412	0.016	1.014 (1.003–1.025)

CI, confidence interval; ECI, elasticity contrast index; ES, elasticity scores; LNM, lymph node metastasis; OR, odds ratio; PTC, papillary thyroid carcinoma; SD-LS, S-Detect in the longitudinal plane; Std, standard error; US, ultrasound.

leaving a gap in the clinical US arena, where intuitive descriptions are scarce. To bridge this gap, our study presents a fresh perspective that holds substantial clinical significance and value.

This groundbreaking study marks the first attempt to quantify the angle between the maximum diameter of thyroid nodules. It delves into the potential of orientational quantification, leveraging conventional US and S-Detect under multi-plane scanning, as an independent predictor for cervical LNM in PTC, beyond just the aspect ratio. The aggressive nature of malignant thyroid tumor cells, characterized by their heightened invasive and proliferative abilities, spreading along tissue spaces, blood vessels, and lymphatic vessels. This results in pronounced growth along specific axes, giving rise to irregular nodular contours that often obscure boundaries on conventional US imaging. Neovascularization and matrix metalloproteinases (MMPs) promote rapid longitudinal growth through vessel formation and extracellular matrix degradation (29). Epithelial-mesenchymal transition (EMT), a biological process that bolsters cancer cell motility, reinforces this longitudinal migration, elongating the nodular shape even further (30). The multivariate analysis conducted in our study demonstrated that both age (<55 years) and nodule size (≥1 cm) diameter served as significant predictors for LNM in PTC, suggesting a possible correlation with elevated metastatic risk. While our study emphasizes imaging features, these clinical parameters maintain significant importance in the predictive model, aligning with findings from previous studies (31-33). Our findings underscore the statistical significance of the quantified angle of the maximum diameter direction, as identified

by S-Detect in the longitudinal plane, in both univariate and multivariate logistic analyses (both P<0.05). Notably, a cutoff value of −16.35° emerges, signifying that the deepest extremity of the maximum diameter line subtly inclines towards the patient's cranial aspect. It exceeds conventional US in Sen, Spe, PPV, and NPV, and Acc for predicting cervical LNM in PTC. This suggests that S-Detect exhibits greater precision than sonographers in identifying the maximum diameter of nodules, and the orientational quantification in longitudinal scanning offers a superior predictive value. Studies have revealed that when the maximum diameter of thyroid nodules is nearly parallel to the skin surface or the deep end inclines slightly towards the patient's body, the interaction with surrounding blood vessels and lymphatic systems increases, markedly elevating the risk of CLNM. The cut-off value of −16.35° as a predictive indicator underscores the pivotal role of nodule orientation in assessing metastatic potential, whereas absolute value conversion and lateral lobe position conversion values are not statistically significant (both P>0.05). A study involving 823 PTC patients with LNM showed that an aspect ratio ≥1 is more common in lateral lobe PTC than in isthmus PTC, but the rate of LN dissection is significantly higher in the isthmus PTC group (P<0.001) (34). Recognizing the relatively modest sample size of this study, we aim to continue investigating whether orientational quantification has consistent predictive performance across different thyroid lobe groups.

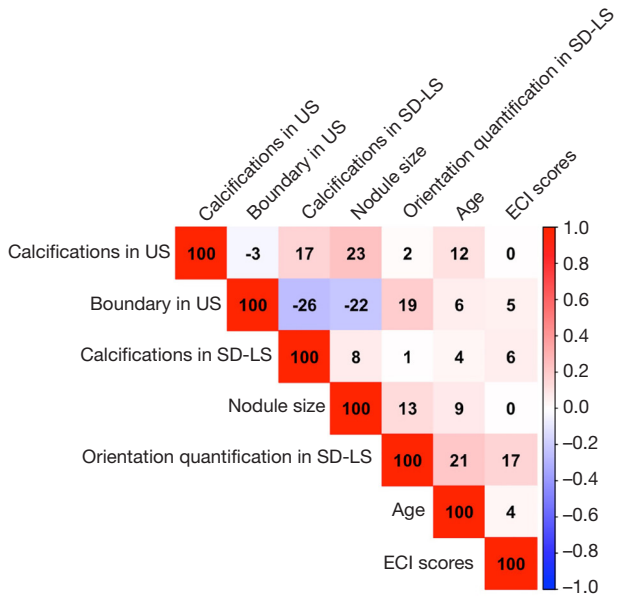

Figure 2 Correlation coefficients in multivariate logistic regression. ECI, elasticity contrast index; SD-LS, S-Detect in the longitudinal plane; US, ultrasound.

Currently, the predictive value of UE for LNM in PTC remains a subject of ongoing debate. Jiang *et al.* reported that the elasticity scores (five-point method) are significantly

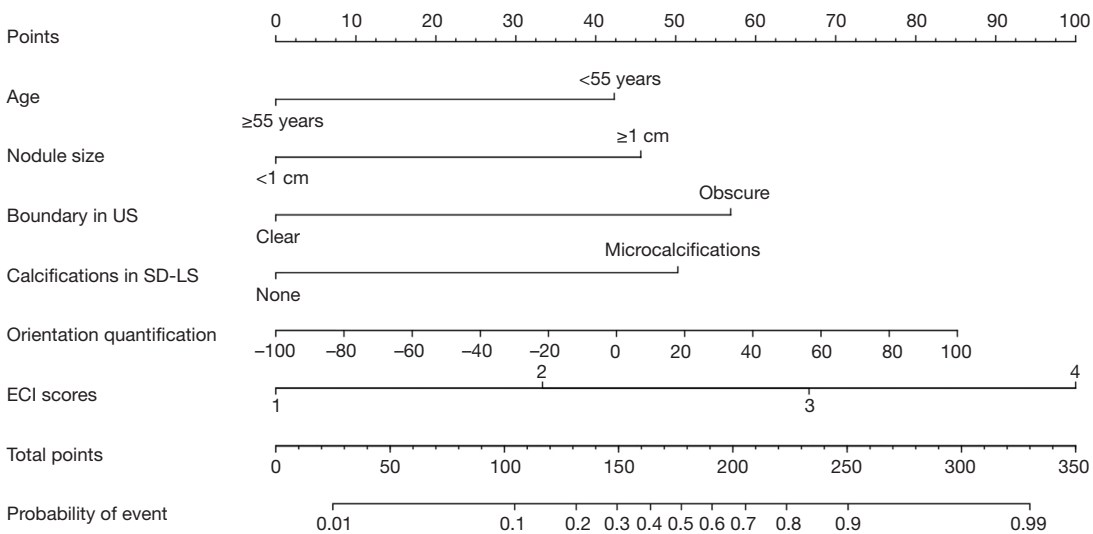

Figure 3 Nomogram on multivariate regression analysis. ECI, elasticity contrast index; SD-LS, S-Detect in the longitudinal plane; US, ultrasound.

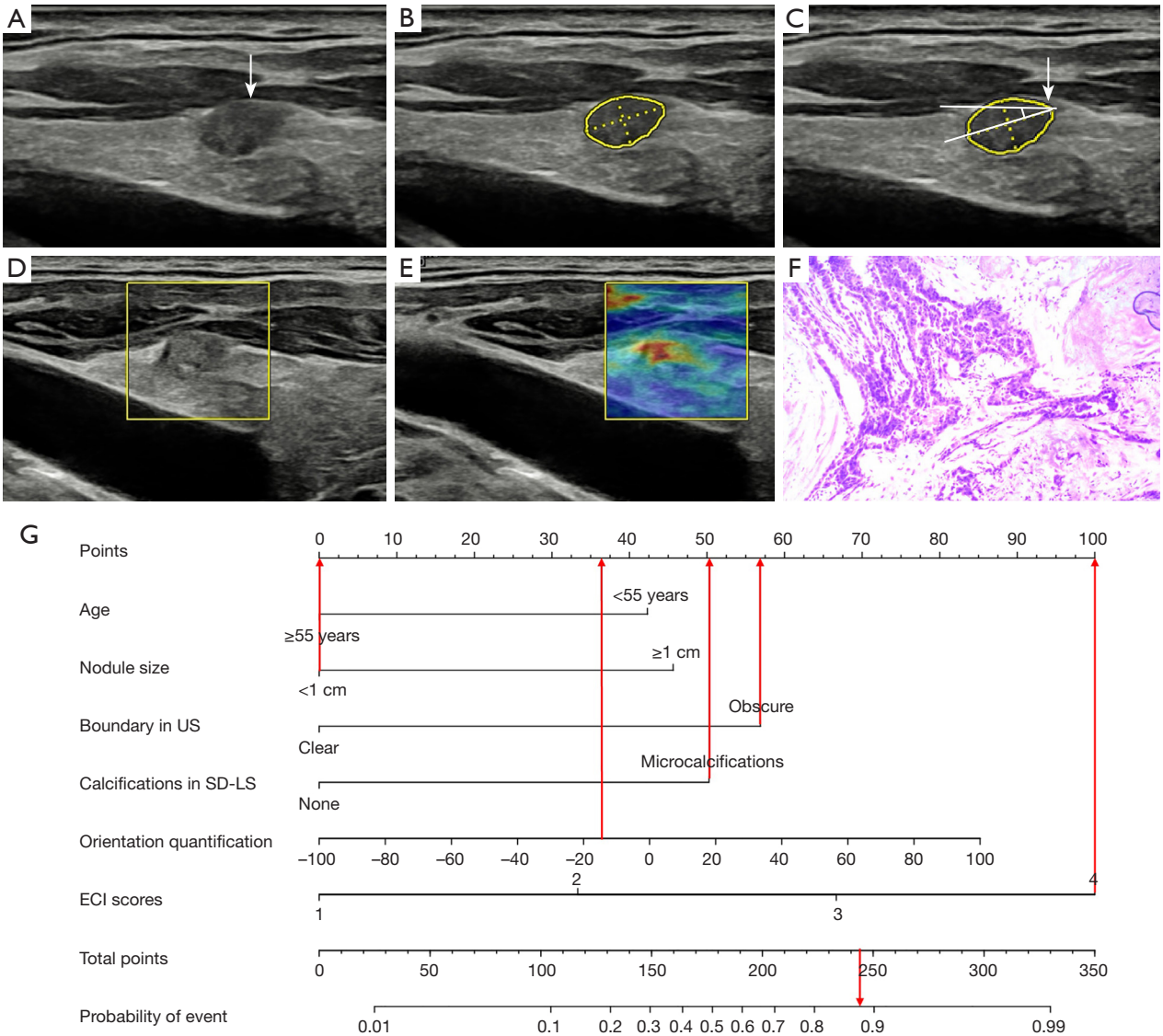

Figure 4 Male, 59 years old (0 point), PTC with LNM, maximum nodule diameter 0.66 cm (0 point), obscure in boundary in US (57 points), calcifications in SD-LS are microcalcifications (51 points), ECI scores 4 (100 points), retrospective longitudinal S-Detect measurement of maximum diameter angle −16.2° (36 points), total score approximately 244 points, the probability of LNM in this patient is around 88%. (A) Conventional US in the longitudinal plane (arrow). (B) S-Detect in the longitudinal plane. The yellow circle represents the nodule ROI region automatically outlined by S-Detect. (C) The angle measured in the longitudinal plane by S-Detect is −16.2° (arrow). The yellow circle represents the nodule ROI region automatically outlined by S-Detect. (D) Select the nodule cross-section and determine the sampling frame. The yellow box represents the ECI region outlined by the examining doctor. (E) ECI elastography (score 4). (F) Pathology paraffin shows PTC [magnification: 100×; stain: hematoxylin and eosin (HE)]. (G) Variable factors corresponding nomogram scores. ECI, elasticity contrast index; LNM, lymph node metastasis; PTC, papillary thyroid carcinoma; HE, hematoxylin and eosin; ROI, region of interest; SD-LS, S-Detect in the longitudinal plane; US, ultrasound.

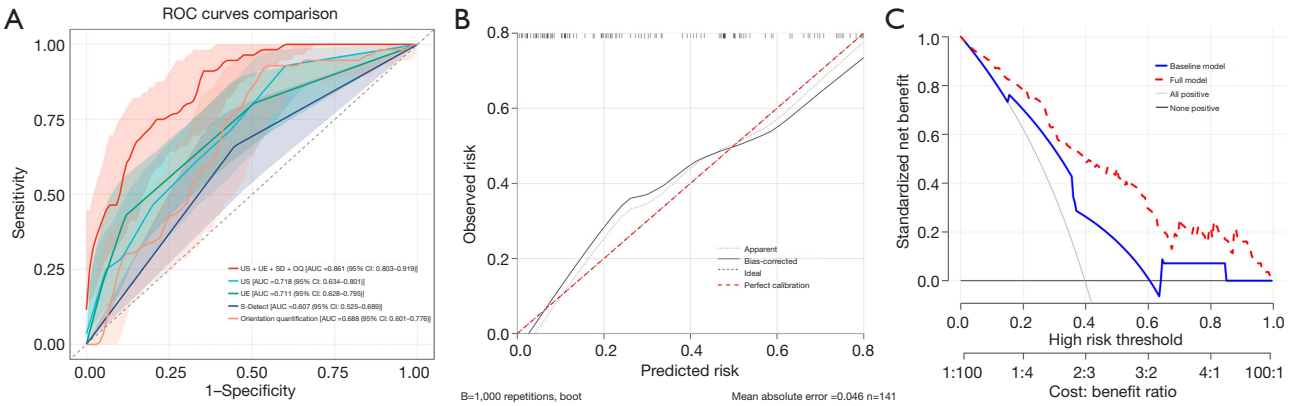

Figure 5 ROC curves, calibration curve and decision analysis curve analysis. (A) ROC curves comparison of different models. The US + UE + SD + OQ model showed the highest AUC of 0.861 (95% CI: 0.803–0.919), followed by US model (AUC =0.718; 95% CI: 0.634–0.801), UE model (AUC =0.711; 95% CI: 0.628–0.795), S-Detect model (AUC =0.607; 95% CI: 0.525–0.689), and orientation quantification model (AUC =0.688; 95% CI: 0.601–0.776). (B) The calibration curve of the nomogram model shows that the predicted results align almost perfectly with the actual cervical LNM situations, no significant statistical difference the goodness-of-fit (χ^2=3.271; P=0.926), indicating good consistency. (C) The decision curve of nomogram prediction model shows a good net benefit when the threshold probability is between 1.5% and 99.5%. AUC, area under the curve; CI, confidence interval; LNM, lymph node metastasis; OQ, orientation quantification; ROC, receiver operating characteristic; SD, S-Detect; UE, ultrasound elastography; US, ultrasound.

important in diagnosing the hardness of metastatic LNs (P<0.05; OR =4.901; 95% CI: 1.131–1.861) (35). However, studies conducted by Hong *et al.*, Xu *et al.*, and Wang *et al.* have concluded that elasticity scores (four-point, five-point, six-point methods) are not significant predictors of CLNM in PTC (36-38). Conversely, Moon *et al.* found no significant difference in elasticity scores between the metastatic and non-metastatic groups (P=0.362), but identified the elasticity scores as an independent predictor of extrathyroidal extension (OR =5.060; 95% CI: 1.565–16.358) (12). In this study, we found that under ECI, the four-point elasticity scores is an independent predictor (score 3, score 4, both P<0.05; OR =2.781; 95% CI: 1.699–4.552). Multivariate analysis revealed that microcalcification identified by S-Detect in the longitudinal plane is the best predictor for the metastatic group (OR =4.159; 95% CI: 1.545–11.199). The potential explanation for this observation is that, in order to accurately measure the orientational quantification angle and reduce errors, we included large calcifications and major artifacts in the exclusion criteria to obtain complete and clear images of nodule edges, which resulted in the inclusion of 141 nodules that were either non-calcified or microcalcified, thus introducing some selection bias. Microcalcifications composed of calcium phosphate and hydroxyapatite are frequently found in necrotic and degenerative areas and are highly associated with PTC, appearing as small, echogenic points on US images with high elasticity scores. Large calcifications, typically arising from calcium salt deposits during long-term chronic degeneration, present as larger plaque like or ringlike echogenic reflections. However, their hardness on US images is less distinct than that of microcalcifications. As a result, in this study, the predictive factor weight (OR) of microcalcifications identified by S-Detect in the longitudinal plane is comparatively higher when contrasted with findings reported in other literature.

Compared to a single model, the combined model of conventional US, UE, S-Detect, and orientational quantification exhibits the most outstanding overall performance, featuring AUC (95% CI), NPV, and Acc that all surpass those of single models. This indicates that the nomogram model we have constructed has high diagnostic reliability, low misdiagnosis risk, and high screening efficacy, thereby providing robust recommendations for clinical decision-making. Furthermore, compared to other studies' combined models for predicting cervical LNM in PTC, the four examination methods in this study are relatively simple to perform, time-efficient, and exhibit a reduced level of dependent on the examiner's experience and judgment.

Several limitations merit consideration in this study. Firstly, it is a retrospective single-center study with a small sample size, and the uniform clinical evaluation standards

influenced the results, with 97 cases (68.8%) having nodules with a maximum diameter <1 cm, possibly leading to selection bias. While our statistical analysis revealed promising predictive capabilities, our relatively limited sample size might not comprehensively represent the full spectrum of clinical presentations, especially regarding the inadequate representation of cases with atypical imaging features, potentially impacting both the universality of our findings and the robustness of our predictive model. Consequently, further external validation through prospective investigations across diverse populations and multiple medical centers is warranted. Secondly, as US is operator-dependent, this study only involved two mid-level US doctors with comparable experience, who retrospectively evaluated the consistency of S-Detect's region of interest (ROI) area and orientational quantification, without assessing inter-operator variability among US physicians of different experience levels. Lastly, the study's reliance on a single machine learning method to identify the maximum diameter as an independent predictive factor necessitates the conduct of prospective studies, ideally involving senior physicians and multiple model groups, to more comprehensively investigate its significance and validity.

Conclusions

Establishing the optimal orientational angle for the evaluation of thyroid nodules provides a new perspective for predicting cervical LNM in PTC. Compared to conventional US, it exhibits equivalent Sen while achieving superior performance in terms of Spe, PPV, NPV, AUC, and net benefit value. The nomogram model in this study, which integrates conventional US, UE, S-Detect, and orientational quantification for predicting the risk of CLNM in PTC patients, can provide valuable reference information for clinical prognosis evaluation.

Acknowledgments

We sincerely thank Hou-Wei Chen for her assistance in the English writing of this manuscript.

Footnote

Reporting Checklist: The authors have completed the STROBE reporting checklist. Available at https://qims.amegroups.com/article/view/10.21037/qims-24-1650/rc

Funding: This work was supported by the funding project: Tianshan Young Talent Scientific and Technological Innovation Team: Innovative Team for Research on Prevention and Treatment of High-incidence Diseases in Central Asia, Project (No. 2023TSYCTD0020) and Guidance Plan Project of the Xinjiang Production and Construction Corps (No. 2023ZD004).

Conflicts of Interest: All authors have completed the ICMJE uniform disclosure form (available at https://qims.amegroups.com/article/view/10.21037/qims-24-1650/coif). The authors have no conflicts of interest to declare.

Ethical Statement: The authors are accountable for all aspects of the work in ensuring that questions related to the accuracy or integrity of any part of the work are appropriately investigated and resolved. The study was conducted in accordance with the Declaration of Helsinki (as revised in 2013). The study was approved by the institutional ethics committee of the First Affiliated Hospital of Shihezi University (No. KJ2024-250-01). Informed consent was taken from all the participants.

References

1. Miranda-Filho A, Lortet-Tieulent J, Bray F, Cao B, Franceschi S, Vaccarella S, Dal Maso L. Thyroid cancer incidence trends by histology in 25 countries: a population-based study. Lancet Diabetes Endocrinol 2021;9:225-34.
2. Cao M, Li H, Sun D, Chen W. Cancer burden of major cancers in China: A need for sustainable actions. Cancer Commun (Lond) 2020;40:205-10.
3. Siegel RL, Miller KD, Wagle NS, Jemal A. Cancer statistics, 2023. CA Cancer J Clin 2023;73:17-48.
4. Lundgren CI, Hall P, Dickman PW, Zedenius J. Clinically significant prognostic factors for differentiated thyroid carcinoma: a population-based, nested case-control study. Cancer 2006;106:524-31.

5. Tong Y, Zhang J, Wei Y, Yu J, Zhan W, Xia H, Zhou S, Wang Y, Chang C. Ultrasound-based radiomics analysis for preoperative prediction of central and lateral cervical lymph node metastasis in papillary thyroid carcinoma: a multi-institutional study. BMC Med Imaging 2022;22:82.
6. Alabousi M, Alabousi A, Adham S, Pozdnyakov A, Ramadan S, Chaudhari H, Young JEM, Gupta M, Harish S. Diagnostic Test Accuracy of Ultrasonography vs Computed Tomography for Papillary Thyroid Cancer Cervical Lymph Node Metastasis: A Systematic Review and Meta-analysis. JAMA Otolaryngol Head Neck Surg 2022;148:107-18.
7. Haugen BR, Alexander EK, Bible KC, Doherty GM, Mandel SJ, Nikiforov YE, Pacini F, Randolph GW, Sawka AM, Schlumberger M, Schuff KG, Sherman SI, Sosa JA, Steward DL, Tuttle RM, Wartofsky L. 2015 American Thyroid Association Management Guidelines for Adult Patients with Thyroid Nodules and Differentiated Thyroid Cancer: The American Thyroid Association Guidelines Task Force on Thyroid Nodules and Differentiated Thyroid Cancer. Thyroid 2016;26:1-133.
8. Takami H, Ito Y, Okamoto T, Onoda N, Noguchi H, Yoshida A. Revisiting the guidelines issued by the Japanese Society of Thyroid Surgeons and Japan Association of Endocrine Surgeons: a gradual move towards consensus between Japanese and western practice in the management of thyroid carcinoma. World J Surg 2014;38:2002-10.
9. Monpeyssen H, Tramalloni J, Poirée S, Hélénon O, Correas JM. Elastography of the thyroid. Diagn Interv Imaging 2013;94:535-44.
10. Hu X, Liu Y, Qian L. Diagnostic potential of real-time elastography (RTE) and shear wave elastography (SWE) to differentiate benign and malignant thyroid nodules: A systematic review and meta-analysis. Medicine (Baltimore) 2017;96:e8282.
11. Liu BJ, Li DD, Xu HX, Guo LH, Zhang YF, Xu JM, Liu C, Liu LN, Li XL, Xu XH, Qu S, Xing M. Quantitative Shear Wave Velocity Measurement on Acoustic Radiation Force Impulse Elastography for Differential Diagnosis between Benign and Malignant Thyroid Nodules: A Meta-analysis. Ultrasound Med Biol 2015;41:3035-43.
12. Moon HJ, Kim EK, Yoon JH, Kwak JY. Clinical implication of elastography as a prognostic factor of papillary thyroid microcarcinoma. Ann Surg Oncol 2012;19:2279-87.
13. Yamashita H, Noguchi S, Murakami N, Toda M, Uchino S, Watanabe S, Kawamoto H. Extracapsular invasion of lymph node metastasis. A good indicator of disease recurrence and poor prognosis in patients with thyroid microcarcinoma. Cancer 1999;86:842-9.
14. Sorrenti S, Dolcetti V, Radzina M, Bellini MI, Frezza F, Munir K, Grani G, Durante C, D'Andrea V, David E, Calò PG, Lori E, Cantisani V. Artificial Intelligence for Thyroid Nodule Characterization: Where Are We Standing? Cancers (Basel) 2022;14:3357.
15. Choi YJ, Baek JH, Park HS, Shim WH, Kim TY, Shong YK, Lee JH. A Computer-Aided Diagnosis System Using Artificial Intelligence for the Diagnosis and Characterization of Thyroid Nodules on Ultrasound: Initial Clinical Assessment. Thyroid 2017;27:546-52.
16. Sant VR, Radhachandran A, Ivezic V, Lee DT, Livhits MJ, Wu JX, Masamed R, Arnold CW, Yeh MW, Speier W. From Bench-to-Bedside: How Artificial Intelligence is Changing Thyroid Nodule Diagnostics, a Systematic Review. J Clin Endocrinol Metab 2024;109:1684-93.
17. Zhou J, Yin L, Wei X, Zhang S, Song Y, Luo B, et al. 2020 Chinese guidelines for ultrasound malignancy risk stratification of thyroid nodules: the C-TIRADS. Endocrine 2020;70:256-79.
18. Tessler FN, Middleton WD, Grant EG, Hoang JK, Berland LL, Teefey SA, Cronan JJ, Beland MD, Desser TS, Frates MC, Hammers LW, Hamper UM, Langer JE, Reading CC, Scoutt LM, Stavros AT. ACR Thyroid Imaging, Reporting and Data System (TI-RADS): White Paper of the ACR TI-RADS Committee. J Am Coll Radiol 2017;14:587-95.
19. Kwak JY, Han KH, Yoon JH, Moon HJ, Son EJ, Park SH, Jung HK, Choi JS, Kim BM, Kim EK. Thyroid imaging reporting and data system for US features of nodules: a step in establishing better stratification of cancer risk. Radiology 2011;260:892-9.
20. Li J, Li C, Zhou X, Huang J, Yang P, Cang Y, Zhai H, Huang R, Mu Y, Gou X, Zhang Y, Yu J, Liang P. US Risk Stratification System for Follicular Thyroid Neoplasms. Radiology 2023;309:e230949.
21. Li P, Liu Y, Wei T, Wang X, Zhu J, Yang R, Gong Y, Zhao W. Effect and Interactions of BRAF on Lymph Node Metastasis in Papillary Thyroid Carcinoma With Hashimoto Thyroiditis. J Clin Endocrinol Metab 2024;109:944-54.
22. Yu F, Wu W, Zhang L, Li S, Yao X, Wang J, Ni Y, Meng Q, Yang R, Wang F, Shi L. Cervical lymph node metastasis prediction of postoperative papillary thyroid carcinoma before (131)I therapy based on clinical and ultrasound characteristics. Front Endocrinol (Lausanne) 2023;14:1122517.

23. Feng JW, Ye J, Qi GF, Hong LZ, Wang F, Liu SY, Jiang Y. A comparative analysis of eight machine learning models for the prediction of lateral lymph node metastasis in patients with papillary thyroid carcinoma. Front Endocrinol (Lausanne) 2022;13:1004913.
24. Guang Y, Wan F, He W, Zhang W, Gan C, Dong P, Zhang H, Zhang Y. A model for predicting lymph node metastasis of thyroid carcinoma: a multimodality convolutional neural network study. Quant Imaging Med Surg 2023;13:8370-82.
25. Riley RD, Ensor J, Snell KIE, Harrell FE Jr, Martin GP, Reitsma JB, Moons KGM, Collins G, van Smeden M. Calculating the sample size required for developing a clinical prediction model. BMJ 2020;368:m441.
26. Choi WJ, Park JS, Koo HR, Kim SY, Chung MS, Tae K. Ultrasound elastography using carotid artery pulsation in the differential diagnosis of sonographically indeterminate thyroid nodules. AJR Am J Roentgenol 2015;204:396-401.
27. Asteria C, Giovanardi A, Pizzocaro A, Cozzaglio L, Morabito A, Somalvico F, Zoppo A. US-elastography in the differential diagnosis of benign and malignant thyroid nodules. Thyroid 2008;18:523-31.
28. Zhang M, Zhang Y, Qiu Y, Wei H, Lyu S. A nomogram based on ultrasound characteristics to predict large-number cervical lymph node metastasis in papillary thyroid carcinoma. Endocr J 2023;70:481-8.
29. Zhang FX, Xu P, Zhang LJ, Fan R, Zhang HX, Liu DH, Liu K, Shen DY. RARγ promotes the invasion and metastasis of thyroid carcinoma by activating the JAK1-STAT3-CD24/MMPs axis. Int Immunopharmacol 2023;125:111129.
30. Liu L, Wu B, Cai H, Li D, Ma Y, Zhu X, Lv Z, Fan Y, Zhang X. Tiam1 promotes thyroid carcinoma metastasis by modulating EMT via Wnt/β-catenin signaling. Exp Cell Res 2018;362:532-40.
31. Zhou L, Zheng Y, Yao J, Chen L, Xu D. Association between papillary thyroid carcinoma and cervical lymph node metastasis based on ultrasonic radio frequency signals. Cancer Med 2023;12:14305-16.
32. Ma B, Chen X, Zhao Z, Yin X, Ji Q, Zhou Y, Ma C, Wang J. Coexisting CLT in PTC is an independent predictor of tumor aggressiveness for patients aged under 55: a retrospective analysis of 635 patients. BMC Endocr Disord 2022;22:55.
33. Wan F, He W, Zhang W, Zhang H, Zhang Y, Guang Y. Application of decision tree algorithms to predict central lymph node metastasis in well-differentiated papillary thyroid carcinoma based on multimodal ultrasound parameters: a retrospective study. Quant Imaging Med Surg 2023;13:2081-97.
34. Fan J, Zhou W, Zhan W, Tao L, Li W, Kuang L. Clinical and Ultrasonographic Features of Papillary Thyroid Carcinoma Located in the Isthmus. Ultrasound Q 2023;39:32-6.
35. Jiang W, Wei HY, Zhang HY, Zhuo QL. Value of contrast-enhanced ultrasound combined with elastography in evaluating cervical lymph node metastasis in papillary thyroid carcinoma. World J Clin Cases 2019;7:49-57.
36. Hong YR, Yan CX, Mo GQ, Luo ZY, Zhang Y, Wang Y, Huang PT. Conventional US, elastography, and contrast enhanced US features of papillary thyroid microcarcinoma predict central compartment lymph node metastases. Sci Rep 2015;5:7748.
37. Wang H, Zhao L, Xin X, Wei X, Zhang S, Li Y, Gao M. Diagnostic value of elastosonography for thyroid microcarcinoma. Ultrasonics 2014;54:1945-9.
38. Xu JM, Xu XH, Xu HX, Zhang YF, Guo LH, Liu LN, Liu C, Bo XW, Qu S, Xing M, Li XL. Prediction of cervical lymph node metastasis in patients with papillary thyroid cancer using combined conventional ultrasound, strain elastography, and acoustic radiation force impulse (ARFI) elastography. Eur Radiol 2016;26:2611-22.

Cite this article as: Xu ZL, Hou JX, Zheng ZH, Deng YQ, Zeng GM, Wang SR, Zhu PS, Kang YF, Du TT, Dong J, Liu W, Li J, Cui XW. Enhancing prediction of cervical lymph node metastasis in papillary thyroid carcinoma through nodule-oriented quantification: combined S-Detect and ultrasound elastography. Quant Imaging Med Surg 2025;15(4):3416-3429. doi: 10.21037/qims-24-1650

